The C-terminal actin-binding domain of talin forms an asymmetric catch bond with F-actin

Leanna M. Owen[a,b], Nicolas A. Bax[b,c], William I. Weis[a,c,d,1], and Alexander R. Dunn[a,b,1]

[a]Biophysics Program, Stanford University, Stanford, CA 94305; [b]Chemical Engineering, Stanford University, Stanford, CA 94305; [c]Department of Structural Biology, Stanford University, Stanford, CA 94305; and [d]Department of Molecular & Cellular Physiology, Stanford University, Stanford, CA 94305

Edited by Thomas Pollard, Molecular, Cellular and Developmental Biology, Yale University, New Haven, CT; received May 19, 2021; accepted December 17, 2021

Focal adhesions (FAs) are large, integrin-based protein complexes that link cells to the extracellular matrix (ECM). FAs form only when and where they are necessary to transmit force between the cellular cytoskeleton and the ECM, but how this occurs remains poorly understood. Talin is a 270-kDa adaptor protein that links integrins to filamentous (F)-actin and recruits additional components during FA assembly in a force-dependent manner. Cell biological and developmental data demonstrate that the third and C-terminal F-actin–binding site (ABS3) of talin is required for normal FA formation. However, purified ABS3 binds F-actin only weakly in solution. We used a single molecule optical trap assay to examine how and whether ABS3 binds F-actin under physiologically relevant mechanical loads. We find that ABS3 forms a catch bond with F-actin when force is applied toward the pointed end of the actin filament, with binding lifetimes >100-fold longer than when force is applied toward the barbed end. Long-lived bonds to F-actin under load require the ABS3 C-terminal dimerization domain, whose cleavage has been reported to regulate FA turnover. Our results support a mechanism in which talin ABS3 preferentially binds to and orients actin filaments with barbed ends facing the cell periphery, thus nucleating long-range order in the actin cytoskeleton. We suggest that talin ABS3 may function as a molecular AND gate that allows FA growth only when sufficient integrin density, F-actin polarization, and mechanical tension are simultaneously present.

talin | focal adhesion | catch bond | F-actin

Precise and dynamically regulated force transmission between cells and the extracellular matrix (ECM) is a requirement for cell migration, tissue repair, and, more broadly, the construction of multicellular animal life. Adhesion to the ECM is mediated in large part by integrins, a family of heterodimeric transmembrane proteins that assemble into large adhesion complexes, here referred to generically as focal adhesions (FAs). FA assembly is precisely controlled, such that FAs form only when and where they are necessary to transmit force between the cytoskeleton and the ECM. However, the mechanism by which mechanical force regulates FA nucleation and growth remains poorly understood.

The connection between integrins and the actin cytoskeleton is mediated in large part by talin, a 270-kDa protein that directly binds integrins, F-actin, and other FA components (Fig. 1*A*) (1). Talin possesses three F-actin–binding sites, termed ABS1 to 3. In addition, the talin rod domain is constructed of a series of helical bundle domains that unfold under loads of 5 to 25 pN (2–4) to expose multiple binding sites for the F-actin–binding protein vinculin (5), which is thought to reinforce the adhesion.

Despite the multiple direct and indirect (through vinculin) interactions of talin with F-actin, binding by the C-terminal ABS3 to F-actin is essential for its biological functions (6). ABS3 consists of a five-helix bundle along with an isolated C-terminal alpha helix that mediates antiparallel homodimerization (7–9). ABS3 mutations that disrupt F-actin–binding hinder the initial stages of adhesion formation (10–12) as well as subsequent FA assembly (11–14), cell spreading and polarization (12, 13), and flow-dependent force transmission at adhesions in the lamellipodia (15). *Drosophila* with ABS3 mutations that disrupt F-actin–binding show defects in germband retraction resembling talin-null embryos as well as defects in embryonic muscle–tendon attachment and epithelial sheet adhesion in the adult wing (16, 17). Despite its functional importance, ABS3 binds F-actin only weakly in cosedimentation assays (8, 18–20). A pioneering study in live cells was interpreted to indicate that talin forms a weak, 2-pN slip bond to F-actin that required ABS3 (10). However, to our knowledge, it is not known how, or even whether, mechanical load may affect the stability of the ABS3–F-actin bond.

Results

We used a previously described single-molecule assay (21, 22) to characterize the binding of human ABS3 (human talin-1 residues 2,293 to 2,541 expressed as a HaloTag fusion protein) to F-actin (Fig. 1*B*). We first characterized this interaction in the absence of externally applied load on the actin-ABS3 bond (Fig. 1 *C* and *D* and *SI Appendix*, Fig. 1) and observed only short ABS3–F-actin bond lifetimes with a mean of 47^{52}_{43} ms (90% CI) (Fig. 1*E*). In contrast, in the presence of biologically relevant loads (Fig. 1*F* and *SI Appendix*, Figs. 2 and 3), we observed stable binding of ABS3 to actin, with bond lifetimes in the tens and sometimes hundreds of seconds (Fig. 1*G*).

Significance

Talin is a mechanosensitive adaptor protein that links integrins to the actin cytoskeleton at cell–extracellular matrix adhesions. Although the C-terminal actin-binding domain ABS3 of talin is required for function, it binds weakly to actin in solution. We show that ABS3 binds actin strongly only when subjected to mechanical forces comparable to those generated by the cytoskeleton. Moreover, the interaction between ABS3 and actin depends strongly on the direction of force in a manner predicted to organize actin to facilitate adhesion growth and efficient cytoskeletal force generation. These characteristics can explain how force sensing by talin helps to nucleate adhesions precisely when and where they are required to transmit force between the cytoskeleton and the extracellular matrix.

Author contributions: L.M.O., N.A.B., W.I.W., and A.R.D. designed research; L.M.O. and N.A.B. performed research; L.M.O. and A.R.D. contributed new reagents/analytic tools; L.M.O. analyzed data; and L.M.O., W.I.W., and A.R.D. wrote the paper.

The authors declare no competing interest.

This article is a PNAS Direct Submission.

[1]To whom correspondence may be addressed. Email: bill.weis@stanford.edu or alex.dunn@stanford.edu.

This article contains supporting information online at http://www.pnas.org/lookup/suppl/doi:10.1073/pnas.2109329119/-/DCSupplemental.

Published March 4, 2022.

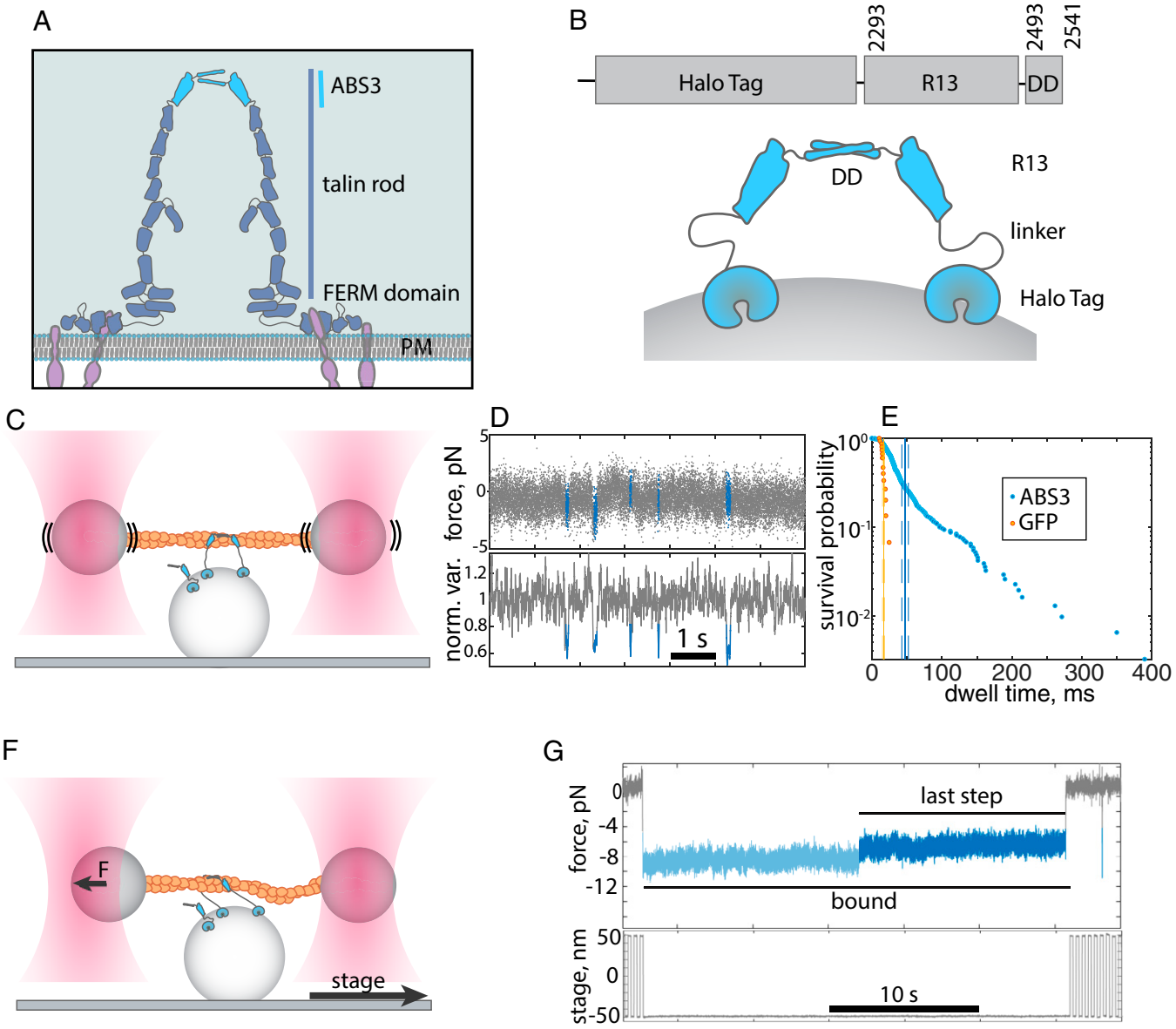

Fig. 1. Binding of talin-1 ABS3 to actin is stabilized by force. (*A*) Cartoon of two full-length talin molecules (blue). Talin is composed of an N-terminal FERM domain that binds the plasma membrane (PM) and β-integrin tails (lavender), a central rod region, and a C-terminal actin-binding domain ABS3 (teal). (*B*) ABS3 construct used in these experiments. ABS3 (Rod domain 13, R13, with DD) was expressed as a HaloTag fusion protein for oriented surface attachment. The DD mediates antiparallel dimerization (8). (*C*) No-load three-bead optical trap experimental setup. ABS3 (light blue) is immobilized via an N-terminal HaloTag domain on a microscope coverslip sparsely decorated with 1.5-μm-diameter platform beads. A single actin filament (orange) is held between two optically trapped 1-μm-diameter beads. The microscope stage is positioned such that a platform bead is positioned underneath the actin filament. (*D*) Sample trace of trapped beads to detect binding of ABS3 to F-actin. In the absence of applied load, ABS3 binding to F-actin is detected as transient drops in the thermal noise of the bead positions due to an increase in the stiffness of the system. (*Top*) The summed force signal of the two trapped beads is plotted in gray in the absence of binding and in blue during a detected binding event. (*Bottom*) Drops in the local, mean-normalized variance in bead position are used to detect binding. (*E*) Binding lifetimes detected with this method. $n = 312$ binding events detected from sampling the ABS3 construct from 1,419 s of recorded data (blue) across nine dumbbells, seven flow cells, and one ABS3 preparation. $n = 15$ binding events detected from sampling an eGFP-coated surface from 2,188 s (orange) across 10 dumbbells and seven flow cells. Mean lifetimes and 90% CI of each mean are demarcated by solid and dashed lines, respectively. (*F*) Loaded three-bead optical trap experimental setup. Same as *C*, except the stage is translated parallel to the actin filament in a trapezoidal wave form. Note that we have depicted the ABS3 dimer as saddling the actin filament, consistent with electron microscopy structures of ABS3 bound to actin (8). (*G*) Force trace and stage displacement as described in *F*. If one or more ABS3 molecules on the platform bead bind to the actin filament while the stage is moving, one of the trapped beads is pulled out of its equilibrium position (demarcated by the blue force trace), thus applying load to the ABS3–F-actin bond. When this occurs, the stage motion is halted until all of the protein complexes unbind, and the trapped beads return to their equilibrium positions. Reported lifetimes are the full length of single step binding events or the last steps (dark blue) of multistep binding events.

Strikingly, we also observed that nearly all long (>0.5 s) binding events associated with a single actin filament were associated with load on only one of the two traps (Fig. 2*A*). The consistency in the preferred direction of long-lived binding events was observed for a given actin filament across multiple platforms, indicating that this behavior did not reflect ABS3

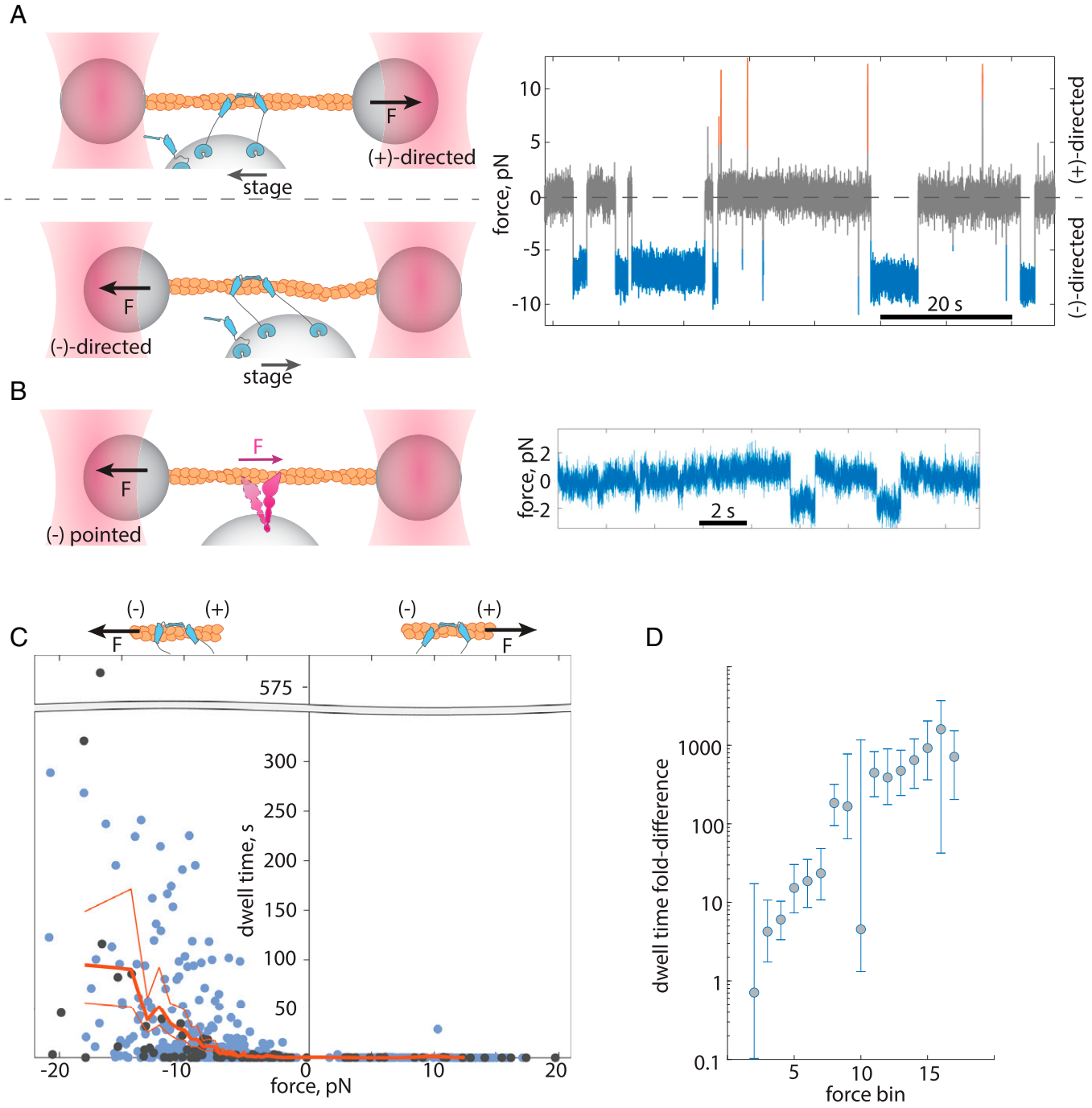

Fig. 2. Talin-1 ABS3 forms a catch bond with F-actin when force is applied toward the pointed end of the actin filament. (*A*) An asymmetry in bond lifetimes is observed for a single actin filament. Load on the right (*Top*) or left (*Bottom*) trapped bead. (*Right*) Sample force trace. Load on the right bead is indicated in orange, while load on the left bead is shown in blue. (*B*, *Left*) A myosin VI construct steps along actin filaments, pulling the bead attached to the (−) end of the filament out of the trap. (*B*, *Right*) Sample myosin trace. In this example, the left bead is attached to the F-actin (−) end. (*C*) ABS3 binding dwell times measured as a function of force. Forces directed toward the pointed (−) end of the filament correspond to negative force values and forces directed toward the barbed (+) end correspond to positive force values. Dark gray: binding lifetimes of events measured in the directionality assay in which the actin filament polarity was explicitly measured for each dumbbell (n = 2 flow cells, n = 3 dumbbells, n = 47 events). Blue: binding dwell times for which the actin filament polarity was statistically inferred. *Orange*: mean dwell times (20 data points per bin), with 90% CI shown in thinner lines (n = 777 binding events, n = 42 dumbbells, n = 18 flow cells, n = 1 ABS3 preparation). (*D*) Mean fold difference in bond lifetime for forces applied toward the pointed versus barbed end of the actin filament, with 90% CI per 1-pN bin.

orientation on the surface. When we reversed the orientation of the actin filament by switching the position of the two beads in the optical traps, the preferred loading direction also switched. This result strongly suggested that the relationship between the polarity of the actin filament and the vector of applied force regulated the stability of the ABS3 to F-actin bond.

We next determined whether long-lived binding events corresponded to load oriented toward the F-actin barbed (+) or pointed (−) end by using a previously reported assay in which

the polarity of a given actin filament is determined using the activity of a myosin VI construct (Fig. 2*B*) (22). (Myosin VI is a non-muscle myosin that moves toward the (−) end of F-actin.) ABS3 binding events longer than 0.48 s only occurred when force was applied toward the F-actin pointed (−) end (Fig. 2*C*). This asymmetry was so striking that we could infer the polarity of actin filaments in previous datasets with high confidence and in so doing quantify force-binding lifetime relationships relative to actin filament polarity (Fig. 2*C*). The difference in binding lifetimes was most striking for forces above 10 pN for which the difference in lifetimes was >100-fold (Fig. 2*D*). Only 125/777 (17%) of the detectable binding events occurred under (+) end–directed loads, suggesting that the measured asymmetry in lifetimes constitutes a lower limit.

To gain insight into the molecular mechanism of catch bond formation, we investigated the survival probabilities of bonds within single force bins. Only forces directed toward the pointed end resulted in sufficient binding events for analysis. We observed that the distribution of forces within each 1-pN bin fit better to a biexponential decay than a single exponential decay (*SI Appendix*, Fig. 4), indicating that there were at least two bound states with different characteristic bond lifetimes at each force (23).

The C-terminal dimerization domain (DD) of ABS3 is required for actin cosedimentation and for the function of ABS3 in vivo (8, 9, 16, 17), and antiparallel ABS3 dimers are observed to wrap around actin filaments when imaged by electron microscopy (8). To determine how this domain contributes to F-actin binding, we created a construct containing talin residues 2,293 to 2,493 that lacked the C-terminal DD termed ABS3ΔDD (Fig. 3*A* and *SI Appendix*, Fig. 5). Consistent with earlier reports, this construct cosedimented with F-actin weakly (*SI Appendix*, Fig. 6*A*). Moreover, we detected no binding events in the optical trap assay longer than 32 ms using the low-force assay (*SI Appendix*, Fig. 6*B*) and no binding under load that could be differentiated from negative controls.

The lack of detectable binding by ABS3ΔDD in the optical trap assay suggested two nonexclusive possibilities for the role of the DD: the DD contributes to the strong binding of a single ABS3 to F-actin, and/or the recruitment of two ABS3 domains is required for binding under load. To distinguish between these possibilities, we first more closely examined the dimerization of ABS3, which had been reported to form a constitutive dimer (25). We used a fluorescence polarization assay to characterize the association of ABS3 with a fluorescently tagged DD peptide (amino acids 2,494 to 2,541). The association of these fragments was reversible, and quantification of the data yielded a dissociation constant $K_D = 1.9 \pm 0.2$ μM (Fig. 3*B*). Multimicromolar K_D values were also estimated for the ABS3 construct based on size-exclusion (SEC) multiple angle light scattering and native polyacrylamide gel electrophoresis experiments (*SI Appendix*, Fig. 7). In our hands, ABS3 dimerization is a dynamic equilibrium at micromolar concentrations.

Next, we created two constructs, termed N-terminal dimer (NTD)-ABS3 and NTD-ABS3ΔDD, in which split GFP (26) was used to make stable dimers of either ABS3 or ABS3ΔDD (Fig. 3*A*). NTD-ABS3ΔDD displayed some F-actin binding in the cosedimentation assay (*SI Appendix*, Fig. 6*A*). NTD-ABS3ΔDD also bound actin in the optical trap in the absence of load with a lifetime of 59^{74}_{46} ms. We observed no binding events longer than 0.8 s in the presence of applied force (*SI Appendix*, Fig. 8). Furthermore, no single actin filament sampled resulted in more than one binding event longer than 0.5 s, making the determination of the long-binding direction infeasible for this dataset. Thus, N-terminal dimerization alone was not sufficient to rescue long-lived, polarized binding in the presence of load.

For NTD-ABS3, forced N-terminal dimerization slightly increased no-load binding in the optical trap assay (*SI Appendix*, Fig. 6*B*) but did not significantly alter binding in the presence of load (Fig. 3*C*). This degree of similarity suggests that ABS3 also forms stable, load-bearing bonds to F-actin only when its C-terminal dimerization domain is present. Although it must be interpreted with care, we also did not observe substeps for the dissociation of ABS3 or NTD-ABS3 from F-actin, which if present would provide evidence for sequential unbinding of individual ABS3 domains. In total, a reasonable interpretation is that 1) definitively monomeric ABS3 (ABS3-ΔDD) binds F-actin only transiently under load, 2) the DD is required for stable F-actin binding under load, and 3) each dissociation step we observe reflects the coordinated detachment within our temporal resolution of an ABS3 dimer from F-actin. This is consistent with electron microscopy data in which antiparallel ABS3 dimers saddle actin filaments, but no ABS3 monomers are reported to bind (8). How the DD's intrinsic actin-binding activity and its C-terminal dimerization dynamics contribute to ABS3's load-dependent binding behavior has yet to be determined. Interestingly, 6 to 10 pN of force, which in our experiments yields mean binding lifetimes of ∼10 s, would correspond to 3 to 5 pN of load per individual talin dimer half. This value is in good accord with measurements of typical loads borne by integrins in living cells (27) and by talin in proximity to ABS3 (28).

Discussion

Previous studies indicate that the talin-binding partner vinculin forms a directional catch bond with F-actin: like talin, the bond between vinculin and F-actin is stabilized when load is oriented toward the pointed end of the actin filament (22). However, both the force dependence and directional preference of ABS3 are extreme—the mean measured lifetimes and the actin polarity preference each increase more than 100-fold under load, enhancements that are ∼10-fold larger than those observed for vinculin. Indirect evidence suggests that talin ABS3 and vinculin may act in concert: knockout of vinculin worsens ABS3 mutant phenotypes in mammalian cells in culture and in *Drosophila* (17), and expression of constitutively active vinculin can compensate for ABS3 disruption in cell culture (14). Whether the talin ABS1 and ABS2 domains and, more broadly, the many other F-actin–binding proteins present at FAs show similar directional sensitivity is not known. However, at a conceptual level, this requires only a binding interaction with F-actin that is asymmetric with respect to the intrinsic polarity of the actin filament as, for example, is seen in the electron microscopy structures of ABS3 and the vinculin F-actin–binding domain bound to F-actin (8, 29). Based on these observations, it is interesting to speculate that asymmetric regulation of dissociation rates by force may be a general property of protein–actin bonds.

How exactly cells regulate the number, size, and placement of FAs has been unclear. As a partial answer, we speculate that ABS3 may function as a molecular AND gate that limits the formation of FAs to highly specific circumstances (Fig. 3*D*). As suggested previously, it is plausible that integrins must be of sufficient local areal density to anchor talin dimers at both *N* termini (30, 31). Furthermore, our results show that substantial, >5-pN loads are required for ABS3 to form long-lived bonds to F-actin. This condition requires that load-bearing connections between the ECM, integrin, and talin are intact and that the proximal ECM is sufficiently stiff to resist cell-generated forces. Finally, load must be oriented toward the F-actin pointed end. This stabilizes oriented F-actin that is under load due to either barbed-end polymerization forces or tension generated by nonmuscle myosin II while allowing misoriented F-actin to escape.

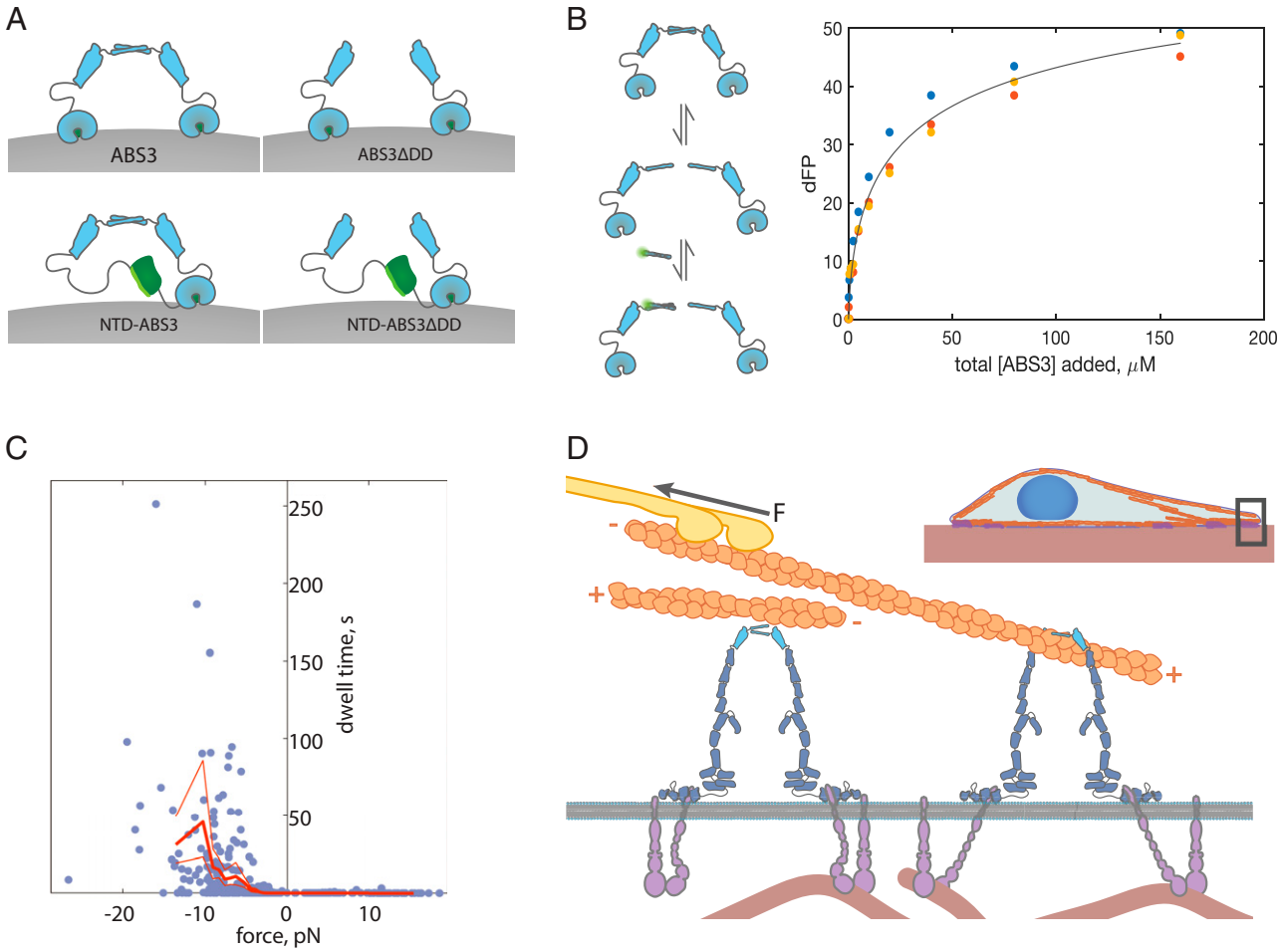

Fig. 3. The C-terminal DD is required for F-actin binding under load. (*A*) The constructs used in this study (see text). The ABS3 construct used in this study contains an N-terminal HaloTag for surface attachment. NTD is formed from the fusion of a split GFP (green). (*B*) Fluorescence polarization assay used to determine the dimer affinity. DD peptide labeled with Oregon Green was held at a constant 25 nM concentration, and the fluorescence polarization was assayed as ABS3 was titrated. Fits to this data resulted in an estimated $K_d = 1.9 \pm 0.2$ μM for dimer formation (gray curve). Data points are colored by replicate. (*C*) Force–lifetime plots of binding events detected for the NTD-ABS3 construct (lavender) with mean lifetime (plotted in thick orange) and CI on the mean (plotted in thin orange) (20 data points per bin). $n = 386$ binding events, $n = 18$ dumbbells, $n = 8$ flow cells, $N = 2$ NTD-ABS3 preparations. (*D*) Model: Talin ABS3 only binds actin when the ECM–integrin–talin force transmission pathway is intact, and actin is under pointed-end–directed load. [Integrin cartoon modified from previous publication (24).] Consistent with electron microscopy data, talin is depicted as wrapping around actin filaments during strong binding (8).

Simulation suggests that the resulting polarization of F-actin can potentially drive cellular-scale organization of the actin cytoskeleton to generate efficient traction and produce directional cell migration (22, 32, 33). We therefore propose that the F-actin–binding properties of ABS3 have evolved to limit FA formation to when and where a force-transmitting anchorage between the cytoskeleton and the ECM is required. Further work is required to test this hypothesis with in vivo experiments and to test whether a similar form of autoregulation may apply to other cellular adhesion complexes.

Our assay design uses fast ramp loading at ∼3,000 pN · s^{-1} followed by constant stage position because this makes subsequent data analysis and model building more straightforward than in the case of experiments carried out with time-varying loads. Relatively few data comment directly on how talin ABS3 may be loaded in vivo. F-actin retrograde flow rates vary between and within cells, with some studies reporting flow rates ranging from 10 to as high as 600 nm · s^{-1} (34). The latter velocity is comparable to that at which non-muscle myosin IIA is predicted to translocate F-actin at physiological temperature and low load (35). The stiffness of the molecular linkages that anchor talin ABS3 is not certain, but a reasonable value based on the stiffness of the talin rod domain is ∼1 pN · nm^{-1}, yielding predicted in vivo loading rates ranging from 10 to 600 pN · s^{-1}. The properties of ABS3 may thus allow it to capture and anchor F-actin undergoing retrograde flow, consistent with the observation that ABS3 mutations that disrupt actin binding also prevent retrograde flow-dependent force transfer to the talin rod and talin-dependent slowing of lamellipodial actin flow (15). More broadly, the exponential increase in binding lifetimes with load between 0 and ∼10 pN (*SI Appendix*, Fig. 9) means that repeated interactions with F-actin will eventually result in an encounter in which an ABS3 dimer surpasses a threshold force and becomes stably attached to F-actin. Understanding how the dynamical properties of ABS3 and other F-actin–binding proteins influence the assembly and dynamics of FAs constitutes an interesting target for future investigations.

Materials and Methods

Constructs. The HaloTag-ABS3 expression vector was constructed by inserting the DNA encoding the HaloTag, a linker sequence, and the human talin-1

C-terminal actin-binding domain (amino acids 2,293 to 2,541) into the pPROEX HTa expression vector to generate an in-frame fusion consisting of a 6xHis-tag, HaloTag, 12-residue linker (SGLGGSGGGGSG), and ABS3. The GFP11-ABS3 vector was generated by insertion of the sequence for GFP11 and ABS3 into a pD444-NH: T5-His-ORF, Ecoli-Elec D expression vector to create an in-frame fusion of 6xHis-tag, a (GGSGG)x2 linker, GFP11, (GGSGG)x6, and ABS3. The GFP 1–10 OPT-HaloTag-ABS3 expression vector was generated by insertion of the sequence for GFP 1–10 OPT, HaloTag, and ABS3 into pD444-NH: T5-His-ORF, Ecoli-Elec D to create an in-frame fusion of a 6xHis-tag, GFP 1–10 OPT, (GGSGG)x2, HaloTag, (GGSGG)x4, and ABS3. The HaloTag-ABS3ΔDD expression vector was generated from the HaloTag-ABS3 expression vector by the insertion of two stop codons before amino acid M2494 of the original talin-1 gene. The GFP11-ABS3ΔDD and GFP 1–10 OPT-HaloTag-ABS3ΔDD expression vectors were generated by site-directed mutagenesis of amino acid M2494 of the original talin-1 gene to generate a stop codon in its place.

Protein Preparation. The GFP11-ABS3 and GFP 1–10 OPT-HaloTag-ABS3 (and GFP11-ABS3ΔDD and GFP 1–10 OPT-HaloTag-ABS3ΔDD) were coexpressed in BL21 (DE3) *Escherichia coli* cultures to facilitate split GFP fusion and stabilization (26). All other constructs were expressed in BL21 (DE3) *E. coli* and induced with isopropyl β-D-1-thiogalactopyranoside. Proteins were purified via nickel-nitrilotriacetic acid affinity chromatography, ion exchange, and SEC before flash freezing for later use. Full details in *SI Appendix, Extended Materials and Methods*.

eGFP was purified and labeled with HaloTag Succinimidyl Ester (O4) Ligand (Promega, P6751) as previously described (22). Ligand labeling densities > 1 HaloTag ligand per eGFP were required for activity of the ABS3 construct.

Actin Biotinylation Protocol. F-actin used in the optical trap assay was purified from rabbit skeletal muscle as previously described (36) and then biotinylated with sulfosuccinimidobiotin (Sigma 203118).

Flow Cell Preparation. Nitrocellulose-coated coverslips with attached platform beads and flow chambers were prepared as described previously (21). Halo-tagged ABS3 fusion constructs were attached to the coverslip and platform bead surface via HaloLigand-eGFP nonspecifically adsorbed onto the coverslip and platform bead surfaces. The surface was passivated with 2% Pluronic F-127 (Sigma, P2443) to prevent nonspecific binding of ABS3 or F-actin with the coverslip surface.

Optical trap experiments were performed in "F-buffer" (20 mM Hepes pH 7.1, 50 mM KCl, 2 mM $MgCl_2$, 0.2 mM $CaCl_2$, 1 mM dithiothreitol, 1 mM ATP) supplemented with 1 mg/mL bovine serum albumin (MCLAB UBSA-100), 0.8% glucose, 2.7 kU/mL catalase (Sigma, C40-100 mg), 7.5 U/mL pyranose oxidase (Sigma P4234-250UN), 1 mM Trolox (Fisher Scientific, AC218940010), washed streptavidin-coated polystyrene microspheres (Bangs Laboratories, Inc; CP01004; diluted 1:400 from stock concentration), and 0.2 nM biotinylated actin filaments labeled with rhodamine-phalloidin (Cytoskeleton PHDR1) and 20 μMphalloidin. A more detailed protocol can be found in *SI Appendix, Extended Materials and Methods*.

Flow cells for determining actin filament polarity and preferred direction of ABS3 binding were prepared as described previously (21).

Optical Trap Instrument. The optical trap used was essentially the same as described previously (21, 22, 37). Each trap was operated at a stiffness of 0.10 to 0.20 pN/nm.

Loaded Optical Trap Assay. The flow cell was prepared as described in *Flow Cell Preparation* and mounted on the stage of the optical trap. Streptavadin-coated beads were captured in each of the two optical trap beams, and the stage was steered to tether a single actin filament to the beads at either end to form a dumbbell. The streptavadin beads were moved apart until the actin filament was taut, with ∼1 to 3 pN tension across the filament. The actin filament was brought into close proximity of a platform bead. The stage was then oscillated parallel to the actin filament 40 to 100 nm, with a 10 nm/ms rise/fall rate and a pause of 150 ms to check for displacement of either trapped bead. If displacement was detected, then the stage paused until both beads relaxed to their starting positions before restarting the oscillation.

Calculation of the Net Force on the Talin/F-actin Bond during the Loaded Optical Trap Assay. Force–lifetime data were measured as described previously (21, 22). Briefly, a bead is held in each trap laser, and the positions of the detection lasers are adjusted to center on the trapped beads. A calibration experiment is performed for each trap that relates the signal of the detection laser on the quadrant photodiode (QPD) to the bead position and trap stiffness. An actin filament is then attached to both trapped beads. The trap lasers (and their trapped beads) are separated until the actin filament is taut. Because the actin filament is held taut, the trapped beads no longer occupy their equilibrium positions in the center of the laser traps. The detection laser is then repositioned to center on the trapped beads to ensure the trapped beads remain in the linear range of the detention signal during binding events. The calibration for each trap is applied to the QPD signal to determine a position (in nm) or equivalent force (in pN) for each trapped bead relative to the detection laser. Data are downsampled to 1 kHz using the "decimate" function in MATLAB. The temporal boundaries of binding events were picked with custom software (MATLAB) and verified manually. The net force on the talin/F-actin bond is determined as described previously (22): When a binding event occurs, one of the beads is pulled further from its equilibrium position while the other bead either moves toward or falls into the center of its trap. Net force applied to the ABS3-actin bond is thus calculated by adding the magnitudes of the force change observed for each bead during a binding event, consistent with force balance (22).

Reported force values associated with force–lifetime data are the mean force on the talin/F-actin bond during the binding event (either the single step or last step of multistep events). Binding events less than 20 ms were excluded from all analyses, as these were also observed in a minority of negative controls. Binding events shorter than the 150-ms stage oscillation pause time and longer than 20 ms were detected and reported. Rare binding events that were terminated coincidentally with the onset of stage oscillation (in which the stage erroneously started oscillating before the binding event ended) were excluded from the analysis.

Assignment of Actin Filament Polarity. Actin filament polarity was explicitly determined as described previously for a subset of the data in which flow cells were prepared with a myosin VI construct consisting of porcine myosin VI (residues 1 to 817) and *Archaeoglobus fulgidus* L7Ae (residues 9 to 118) with a C-terminal eYFP (38) on one-half of the flow cell (22). In this case, actin filaments were held above multiple myosin VI platforms, and the direction of myosin force generation was observed. The actin dumbbell was then moved to a location in the flow cell coated with ABS3, and the loaded optical trap assay was performed. Myosin stepping was observed to displace actin filaments in the same direction as strong ABS3 binding, indicating that ABS3 binds stably when force is applied toward the pointed end of the actin filament for dumbbells measured with this assay. Controls are described in *SI Appendix, Extended Materials and Methods*.

Actin filament polarity was inferred for the remainder of the data in which no myosin VI was present. Filament polarity could be reliably determined for dumbbells for which we measured at least two binding events longer than 0.5 s. In these cases, actin filament polarity was assigned such that the longer mean lifetimes were associated with pointed-end–directed forces. Traces corresponding to actin dumbbells that yielded fewer than two long (>0.5 s) events were excluded from analysis for both ABS3 and NTD-ABS3 in the loaded assay, as the orientation of these filaments could not be clearly determined.

No-Load Optical Trap Assay. For the ABS3 and NTD-ABS3 constructs, the flow cell was prepared as for a loaded optical trap assay. A dumbbell was formed as described in *Loaded Optical Trap Assay*, and platform bead positions were assayed for specific binding activity with load. If binding was detected, the last binding event was allowed to terminate, and the stage oscillation was turned off. Without moving the dumbbell or stage, bead displacement data were then collected at a 40-kHz sampling rate.

Because both the ABS3ΔDD construct and eGFP-negative control produced no obvious specific binding in the presence of force, several platform beads in each of several flow cells were assayed at random.

Binding events were annotated from the above dataset as follows: The 40 kHz signal for each bead position was downsampled to 10 kHz, and a running SD for a 1.5-ms window was taken at every point. This SD trace was mean filtered over a 20-ms window, and binding was detected when the mean-filtered SD dipped below 64% of the average mean-filtered SD for the whole trace. Reported binding event length is the duration that the mean-filtered SD trace was continuously below 80% of the average mean-filtered SD for the whole trace.

Fluorescence Polarization Assay. Talin-1 dimerization domain peptide (amino acids 2,494 to 2,541) with an additional C-terminal Gly-Cys (denoted DD-GC) was labeled at the C terminus with Oregon Green 488 Maleimide and purified by running it on a peptide SEC column. The full protocol is described in *SI Appendix, Extended Materials and Methods*.

ABS3 was buffer exchanged into F-buffer at pH 7.2 by running over a Superdex 200 Increase column. Immediately before the fluorescence

polarization assay, ATP was added to a final concentration of 1 mM ATP. ABS3 was diluted in a 384-well plate (ref. no. 3575, Corning) in F-buffer, and labeled DD-GC was added to each well, including a well with no ABS3, to a final concentration of 25 nM labeled DD-GC. The 384-well plate was incubated overnight at 4 °C in the dark, and then fluorescence polarization measurements were made on a Synergy 2 plate reader (BioTek). Data were analyzed by subtracting fluorescence polarization from the control condition (labeled DD-GC with no ABS3) and fit to the equation

$$FP = \frac{B_{max} * M}{K_d + M},$$

where $M = \frac{-1+\sqrt{1+8T/K_d}}{4K_d}$

denotes the undimerized ABS3 in the case of negligible DD-GC, and T is the total amount of ABS3 added. The above equalities assume that K_d is the dissociation constant describing the homodimerization of ABS3 as well as the heterodimerization of ABS3 and DD-GC.

Data Availability. Data plotted in figures have been deposited in GitHub, https://github.com/AlexDunnLab/Talin_ABS3_PNAS_2022 (39).

ACKNOWLEDGMENTS. We thank T. Omabegho and P. V. Ruijgrok of the Bryant Lab (Stanford University) for providing the myosin VI protein construct. N.A.B. was supported by Training Grant T32 GM007276 from the NIH. L.M.O. was supported by a Graduate Research Fellowship from the NSF. Research reported in this publication was supported by a HHMI Faculty Scholar Award (A.R.D) as well as NIH Grant R01GM114462 to W.I.W. and A.R.D, R35GM130332 to A.R.D., and R35GM131747 to W.I.W. The contents of this publication are solely the responsibility of us and do not necessarily represent the official views of the National Institute of General Medical Sciences or NIH.

1. B. Klapholz, N. H. Brown, Talin – The master of integrin adhesions. *J. Cell Sci.* **130**, 2435–2446 (2017).
2. A. del Rio *et al.* Stretching single talin rod molecules activates vinculin binding. *Science* **323**, 638–641 (2009).
3. M. Yao *et al.*, The mechanical response of talin. *Nat. Commun.* **7**, 11966 (2016).
4. M. Yao *et al.*, Mechanical activation of vinculin binding to talin locks talin in an unfolded conformation. *Sci. Rep.* **4**, 4610 (2014).
5. A. R. Gingras *et al.*, Mapping and consensus sequence identification for multiple vinculin binding sites within the talin rod. *J. Biol. Chem.* **280**, 37217–37224 (2005).
6. B. T. Goult, J. Yan, M. A. Schwartz, Talin as a mechanosensitive signaling hub. *J. Cell Biol.* **217**, 3776–3784 (2018).
7. S. J. Smith, R. O. McCann, A C-terminal dimerization motif is required for focal adhesion targeting of Talin1 and the interaction of the Talin1 I/LWEQ module with F-actin. *Biochemistry* **46**, 10886–10898 (2007).
8. A. R. Gingras *et al.*, The structure of the C-terminal actin-binding domain of talin. *EMBO J.* **27**, 458–469 (2008).
9. N. Bate *et al.*, Talin contains a C-terminal calpain2 cleavage site important in focal adhesion dynamics. *PLoS One* **7**, e34461 (2012).
10. G. Jiang, G. Giannone, D. R. Critchley, E. Fukumoto, M. P. Sheetz, Two-piconewton slip bond between fibronectin and the cytoskeleton depends on talin. *Nature* **424**, 334–337 (2003).
11. G. Giannone, G. Jiang, D. H. Sutton, D. R. Critchley, M. P. Sheetz, Talin1 is critical for force-dependent reinforcement of initial integrin-cytoskeleton bonds but not tyrosine kinase activation. *J. Cell Biol.* **163**, 409–419 (2003).
12. L. Azizi *et al.*, Cancer associated talin point mutations disorganise cell adhesion and migration. *Sci. Rep.* **11**, 347 (2021).
13. P. M. Kopp *et al.*, Studies on the morphology and spreading of human endothelial cells define key inter- and intramolecular interactions for talin1. *Eur. J. Cell Biol.* **89**, 661–673 (2010).
14. P. Atherton *et al.*, Vinculin controls talin engagement with the actomyosin machinery. *Nat. Commun.* **6**, 10038 (2015).
15. T. P. Driscoll, S. J. Ahn, B. Huang, A. Kumar, M. A. Schwartz, Actin flow-dependent and -independent force transmission through integrins. *Proc. Natl. Acad. Sci. U.S.A.* **117**, 32413–32422 (2020).
16. A. Franco-Cea *et al.*, Distinct developmental roles for direct and indirect talin-mediated linkage to actin. *Dev. Biol.* **345**, 64–77 (2010).
17. B. Klapholz *et al.*, Alternative mechanisms for talin to mediate integrin function. *Curr. Biol.* **25**, 847–857 (2015).
18. M. A. Senetar, S. J. Foster, R. O. McCann, Intrasteric inhibition mediates the interaction of the I/LWEQ module proteins Talin1, Talin2, Hip1, and Hip12 with actin. *Biochemistry* **43**, 15418–15428 (2004).
19. S. J. Franco, M. A. Senetar, W. T. N. Simonson, A. Huttenlocher, R. O. McCann, The conserved C-terminal I/LWEQ module targets Talin1 to focal adhesions. *Cell Motil. Cytoskeleton* **63**, 563–581 (2006).
20. J. Srivastava *et al.*, Structural model and functional significance of pH-dependent talin-actin binding for focal adhesion remodeling. *Proc. Natl. Acad. Sci. U.S.A.* **105**, 14436–14441 (2008).
21. C. D. Buckley *et al.*, The minimal cadherin-catenin complex binds to actin filaments under force. *Science* **346**, 1254211 (2014).
22. D. L. Huang, N. A. Bax, C. D. Buckley, W. I. Weis, A. R. Dunn, Vinculin forms a directionally asymmetric catch bond with F-actin. *Science* **357**, 703–706 (2017).
23. W. Thomas *et al.*, Catch-bond model derived from allostery explains force-activated bacterial adhesion. *Biophys. J.* **90**, 753–764 (2006).
24. L. Zhu *et al.*, Structure of Rap1b bound to talin reveals a pathway for triggering integrin activation. *Nat. Commun.* **8**, 1744 (2017).
25. B. T. Goult *et al.*, The structure of an interdomain complex that regulates talin activity. *J. Biol. Chem.* **284**, 15097–15106 (2009).
26. S. Cabantous, T. C. Terwilliger, G. S. Waldo, Protein tagging and detection with engineered self-assembling fragments of green fluorescent protein. *Nat. Biotechnol.* **23**, 102–107 (2005).
27. S. J. Tan *et al.*, Regulation and dynamics of force transmission at individual cell-matrix adhesion bonds. *Sci. Adv.* **6**, eaax0317 (2020).
28. P. Ringer *et al.*, Multiplexing molecular tension sensors reveals piconewton force gradient across talin-1. *Nat. Methods.* **14**, 1090–1096 (2017).
29. L. Y. Kim *et al.*, The structural basis of actin organization by vinculin and metavinculin. *J. Mol. Biol.* **428**, 10–25 (2016).
30. P. Roca-Cusachs, N. C. Gauthier, A. Del Rio, M. P. Sheetz, Clustering of alpha(5)beta(1) integrins determines adhesion strength whereas alpha(v)beta(3) and talin enable mechanotransduction. *Proc. Natl. Acad. Sci. U.S.A.* **106**, 16245–16250 (2009).
31. M. Schvartzman *et al.*, Nanolithographic control of the spatial organization of cellular adhesion receptors at the single-molecule level. *Nano Lett.* **11**, 1306–1312 (2011).
32. I. Thievessen *et al.*, Vinculin is required for cell polarization, migration, and extracellular matrix remodeling in 3D collagen. *FASEB J.* **29**, 4555–4567 (2015).
33. A. Rahman *et al.*, Vinculin regulates directionality and cell polarity in two- and three-dimensional matrix and three-dimensional microtrack migration. *Mol. Biol. Cell* **27**, 1431–1441 (2016).
34. P. Roca-Cusachs, T. Iskratsch, M. P. Sheetz, Finding the weakest link: Exploring integrin-mediated mechanical molecular pathways. *J. Cell Sci.* **125**, 3025–3038 (2012).
35. N. Hundt, W. Steffen, S. Pathan-Chhatbar, M. H. Taft, D. J. Manstein, Load-dependent modulation of non-muscle myosin-2A function by tropomyosin 4.2. *Sci. Rep.* **6**, 20554 (2016).
36. J. A. Spudich, S. Watt, The regulation of rabbit skeletal muscle contraction. I. Biochemical studies of the interaction of the tropomyosin-troponin complex with actin and the proteolytic fragments of myosin. *J. Biol. Chem.* **246**, 4866–4871 (1971).
37. J. Sung, S. Sivaramakrishnan, A. R. Dunn, J. A. Spudich, Single-molecule dual-beam optical trap analysis of protein structure and function. *Methods Enzymol.* **475**, 321–375 (2010).
38. T. Omabegho *et al.*, Controllable molecular motors engineered from myosin and RNA. *Nat. Nanotechnol.* **13**, 34–40 (2018).
39. L. M. Owen, N. A. Bax, W. I. Weis, A. R. Dunn, Talin_ABS3_PNAS_2022. GitHub. https://github.com/AlexDunnLab/Talin_ABS3_PNAS_2022. Deposited 10 February 2022.